RSC Advances




ROYAL SOCIETY OF CHEMISTRY

www.rsc.org/advances

Cite this: DOI: 10.1039/c0xx00000x

www.rsc.org/xxxxxx

ARTICLE TYPE

# Beneficial Metal Ions Insertion into Dandelion-like MnS with Enhanced Catalytic Performance and Morphology Genetic

**Liwei Mi,*[a,c] Yuanfang Chen,[b] Zhi Zheng,[c] Hongwei Hou,[b] Weihua Chen,*[b] and Shizhong Cui[a]**

***Received (in XXX, XXX) Xth XXXXXXXXX 20XX, Accepted Xth XXXXXXXXX 20XX***

**DOI: 10.1039/b000000x**

Large-scale novel hierarchical dandelion-like MnS was successfully synthesized with manganese complex as a template at mild reaction conditions. A mixture of ethylenediamine and ethylene glycol was used as a solvent. Large-scale manganese complexes were obtained via a one-step reaction; the synthesis was very simple, and the raw materials were inexpensive. The as-prepared MnS was used as a template. The introduction of beneficial metals facilitated the catalytic performance of the as-obtained multiple sulphides. Meanwhile, the morphology genetic between the as-prepared MnS and the multiple sulphides was realized via cation exchange. The composition of the products can be adjusted through the cation exchange at room temperature; meanwhile, the performance of the products was improved by large margin without changing the morphology. The as-prepared products showed highly efficient catalytic properties in degrading dye-containing solutions, such as methylene blue and rhodamine B. This result indicated that the performance of the products could be improved by introducing beneficial metals without changing the morphology.

## Introduction

Industrial wastewater is an environmental pollutant that is predicted to become a major threat to hydrosphere ecosystems, biodiversity, and humans[1–3]. Dye wastewater accounts for a large proportion of industrial wastewater[4–6], which contains recalcitrant toxic substances and threatens aquatic living organisms[7]. To degrade toxic substances in dye wastewater, various physical, chemical, and biological techniques have been developed[8–10], such as adsorption, ozonation, electrochemical, and photochemical degradation[11–13]. However, most of these techniques have limited practical application, high operation costs, and low efficiency. In the $H_2O_2$ catalytic oxidation method, transition metal sulphides, which function as catalysts, release highly reactive hydroxyl radicals, which facilitate the degradation of dye wastewater[14–16]. Therefore, transition metal sulphides have a very important function in the catalytic process.

The micro/nanostructure materials have attracted increasing attention because of their magnetic, electrochemical, lithium-ion battery, and catalytic properties. These materials also have a large specific surface area and numerous active sites[17–26]. For example, Duan and co-workers[27] synthesized a manganese dioxide nanostructure and examined its electrochemical properties. Senapati and co-workers[28] reported a magnetic Ni/Ag core–shell nanostructure from prickly Ni nanowire precursor and evaluated its catalytic and antibacterial activities. Wang et al.[29] synthesized novel tunable highly porous CuO nanorods and fabricated high-rate lithium battery anodes with a long cycle life and a high reversible capacity. Meir and his co-workers[30] reported the chemical, optical, and catalytic properties of noble metal (Pt, Pd, Ag, Au)–$Cu_2O$ core–shell nanostructures grown via a general approach. However, the synthesis of large-scale nanostructured materials remains a challenge because of the complicated operation and limitation in industrial application. In this study, a dandelion-like MnS nanostructure was synthesized and used to degrade dye wastewater at room temperature. The dandelion-like MnS was prepared with manganese complex as a precursor at mild reaction conditions. Large-scale chemical materials, which are inexpensive and easy to obtain, were the raw materials for the synthesis of the manganese complex. Large-scale complexes were obtained via a one-step reaction, and the synthesis was very simple.

To improve the catalytic performance of the as-prepared MnS, this study introduced the metal ions of IB group to the as-prepared MnS via the ion exchange method. Copper ion, a member of the IB group, was reported to be an excellent candidate as a catalyst, which has shown significant performance in recent years[31–34]. For example, Wang and co-workers[35] reported the preparation of various kinds of copper sulphides via a facile approach and their enhanced catalytic activities. Moreover, Yang et al.[36] reported Pt–CuS heterodimers and their selective catalytic activity. The present study explored a new viewpoint to introduce the IB group metal ions into the as-prepared MnS. The experimental results showed that the method made an important contribution to improve catalytic performance. In the IB group, $Cu^{2+}$ and $Ag^{+}$ were chosen as the main subjects of this study because of the gold ion that mainly exists in the

trivalent state, which was not helpful in cation exchange reaction. On the other hand, gold ions are expensive and is therefore uneconomical for massive application. Thus, in our experiments, $Cu^{2+}$ and $Ag^{+}$ were introduced to the as-prepared MnS *via* cation exchange. To deal with the complicated experimental operation including modulation of reaction conditions such as concentration, time, temperature, and the long reaction time, the cation exchange reaction was adopted because of its ability to transform nanostructured materials into other forms easily[37–45]. Moreover, the cation exchange reaction between MnS and $Cu^{2+}$ was conducted at room temperature, which was helpful in keeping the morphology of the as-prepared products. Meanwhile, an analogical effect occurred between the as-prepared MnS and $Ag^{+}$. The mild reaction conditions resulted in the slow introduction of the metal ions to induce a gentle reaction on the original unit structure.

In this paper, we chose MnS as the template to synthesize large-scale dandelion-like MnS nanostructures via the solvothermal method at mild conditions. $MnxCu_{1-x}S$ and $Mn_xAg_{2(1-x)}S$ were then fabricated via cation exchange by introducing beneficial metals to MnS. The cation exchange reaction occurred at room temperature by controlling the reaction time and the reactant concentration, which was helpful to the morphology genetic between the as-prepared MnS and $Mn_xCu_{1-x}S$ and $Mn_yAg_{2(1-y)}S$. $Mn_xCu_{1-x}S$ and $Mn_yAg_{2(1-y)}S$ combined the properties of both materials and maximized their advantages. On one hand, the as-prepared products provided a specific surface area and active site when used as a catalyst, which showed high efficiency in degrading methylene blue (MB) and rhodamine B (RB) and were capable of catalyzing $H_2O_2$ and degrading organic dyes. On the other hand, the degradation efficiency of $Mn_xCu_{1-x}S$ and $Mn_yAg_{2(1-y)}S$ was far higher than that of the as-prepared MnS. In this study, the catalytic performance of the products was improved by regulating the composition without changing the morphology.

## Experiment

### Synthesis and processing

The hierarchical dandelion-like MnS (sample **2**) were prepared by a typical solvothermal method with manganese complexes as template. In a typical synthesis, $Mn(C_2H_3O_2)_2{\cdot}4H_2O$ (5 mmol) and toluene-4-sulfonic acid sodium salt (10 mmol) were put into the 50 mL beaker with 20 mL distilled water. Then, the 1, 10-phenanthroline (5 mmol) and 15 mL absolute ethylenediamine was added to the above-mention solution. The mixed solution was heated to almost boiling; the solution was filtered, after the cooling and the crystallization, the manganese complex (sample **1**) was obtained. Then, manganese complex (1 mmol) and thiourea (0.5 mmol) were dissolved by 11 mL glycol and 5 mL absolute ethylenediamine respectively. Then the mixed solution was stirred for 3 h in a 20 mL Teflon-lined autoclave. Afterwards, the autoclave was heated and maintained 160 °C for 24 h in an electric oven, after the heat treatment, the autoclave was allowed to cool down to room temperature. Then, the as-prepared MnS was washed with distilled water and alcohol several times. The product was dried in an oven at 60 °C for 8 h. The cation exchange was conducted between the as-prepared MnS and $Cu(NO_3)_2{\cdot}3H_2O$ to synthesis the $Mn_{0.77}Cu_{0.23}S$ (sample **3**), $Mn_{0.53}Cu_{0.47}S$ (sample **4**), $Mn_{0.40}Cu_{0.60}S$ (sample **5**), $Mn_{0.33}Cu_{0.67}S$ (sample **6**), $Mn_{0.20}Cu_{0.80}S$ (sample **7**), and $Mn_{0.16}Cu_{0.84}S$ (sample **8**), $Mn_{0.10}Cu_{0.90}S$ (sample **9**), and $Mn_{0.05}Cu_{0.95}S$ (sample **10**) with MnS and $Cu(NO_3)_2{\cdot}3H_2O$ ratio of 1 : 2 for 2 min, 5 min, 10 min, 20 min, 30 min, 40 min, 50 min and 1 h, respectively. Furthermore, using the as-prepared MnS and $AgNO_3$ ratio of 1 : 1, $Mn_{0.80}Ag_{0.40}S$ (sample **11**), $Mn_{0.73}Ag_{0.54}S$ (sample **12**), $Mn_{0.58}Ag_{0.82}S$ (sample **13**), $Mn_{0.53}Ag_{0.94}S$ (sample **14**), $Mn_{0.52}Ag_{0.96}S$ (sample **15**) and $Mn_{0.48}Ag_{1.04}S$ (sample **16**) were synthesized under different reaction time (2 min, 4 min, 5 min, 10 min, 20 min and 30 min) at room temperature, respectively. The post-treatment of these products were the same as that of sample **2**.

### Characterization

X-ray diffraction (XRD) patterns were obtained using a Bruker D8 ADVANCE X-ray powder diffractometer with Ni-filtered Cu-Kα radiation at 40 kV and 20 Ma and scanning step of 0.2 $s^{-1}$. All XRD measurements were conducted within the range of $20° \leq 2\theta \leq 80°$. The morphologies and sizes of as-prepared products were characterized with Zeiss EVO LS-15 scanning electron microscope equipped with an energydispersive X-ray spectroscopy (EDS) system. The structure of as-prepared MnS was recorded with a JEOL JEM-2010 transmission electron microscope (TEM). The ultravioletvisible (UV-vis) spectra were recorded on a PerkinElmer Lambda 35 spectrophotometer in the 200 nm to 1100 nm wavelength range.

### Catalytic activity test

MB and RB were selected as the model chemicals to evaluate the activity of the catalysts. In this work, 0.02 g of as-prepared products as catalyst were combined with MB or RB dye solution (30 mg /L, 30 mL), and the reaction was initiated by 10mL $H_2O_2$. The dissolved solution was stirred under irradiation from a UV lamp (λ=253.7 nm) at room temperature. The MB or RB concentration was determined with a UV-vis spectrophotometer (PerkinElmer Lambda 35). At each sampling time (about 2 min), 3 mL solvent was removed from the MB or RB solution and was immediately used for analysis. After the reaction, the catalyst was removed and washed with distilled water for further reuse.

## Results and discussion

Large-scale hierarchical MnS was synthesized with manganese complex as a precursor in a mixed solvent of ethylene glycol and ethylenediamine for 24 h at mild reaction conditions. In general, a large quantity of metal complex is difficult to synthesize. In this study, toluene-4-sulfonic acid sodium salt and 10-phenanthroline were used to synthesize manganese complex, which are common chemicals with low cost. Large-scale manganese complexes were obtained via a one-step reaction, and the synthesis was very simple. Manganese complex was chosen as a precursor because the complex has several advantages over other templates. Compared with the metal salt, the coordinating ability of the bonds in the metal complex delays the release rate of the central metal ion. In addition, the metal complex has a coordinating ability and the ability of orderly arranging the metal ions[46]. All of the advantages of the metal complex facilitated the control of the

morphology and size of the products. Moreover, the auxiliary ligand in the complex functioned as a reaction-active agent or auxiliary agent after dissociation from the complex. Well-shaped CuS was successfully synthesized using the complex in previous reports[47–48]. Considering the stable structure and good coordination ability of the metal complex, the present study chose manganese complex as a precursor to synthesize large-scale uniform MnS, and this complex facilitated the control of the morphology of the as-prepared MnS.

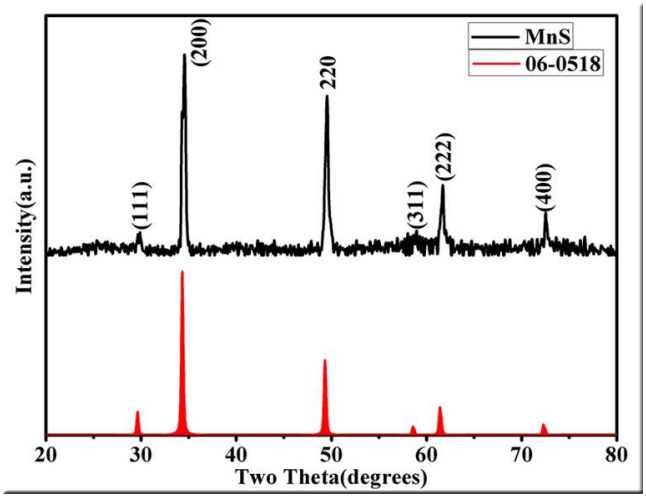


**Fig.1** XRD pattern of as-prepared MnS

Fig. 1 shows the typical XRD pattern of as-prepared needle-like MnS. The pattern indicates that all of the primary diffraction peaks were in good agreement with the standard data for MnS (JCPDS No. 06-0518). This result suggests that the as-prepared MnS had a pure phase. The cell parameters of the products were a = 5.224 Å and c = 5.224 Å. The diffraction peaks located at 29.60, 34.30, 49.30, 58.56, 61.39, and 72.28 corresponded to the directions of 111, 200, 220, 311, 222, and 400, respectively. The strongest direction was the 200 peak, which indicates the preferential growth process. No other phases or impurities was observed in the spectra, which reveal the high-phase purity of the as-prepared MnS. Therefore, uniform dandelion-like MnS was obtained via a simple approach at mild conditions.

Fig. 2 illustrates the morphology of the as-prepared MnS. The low-magnification SEM image of MnS is shown in Fig. 2a. The as-prepared MnS contained large-scale isolated dandelion-like MnS microspheres, which had uniform sizes, and the diameters of the individual needle-like microspheres ranged from 2 μm to 3 μm. The SEM image of large-scale MnS was shown in Fig. S1. In Fig. 2b, each MnS needle-like microsphere included several 3D needle hierarchical structures, which had dandelion-like structures. The thickness of the nano-stick was approximately 20 nm to 30 nm, as shown in Fig. 2c. The as-prepared dandelion-like MnS composed of nano-sticks with a narrow size distribution was believed to improve the catalytic performance because of the large contact area. As presented in Fig. 2d, the high-resolution transmission electron microscopy image was recorded to examine further the crystallographic features of Sample **2**, which shows clear lattice fringes with a d-spacing of 0.462 nm. These features could be indexed to the (220) plane of the MnS crystal (JCPDS No. 06-0518).

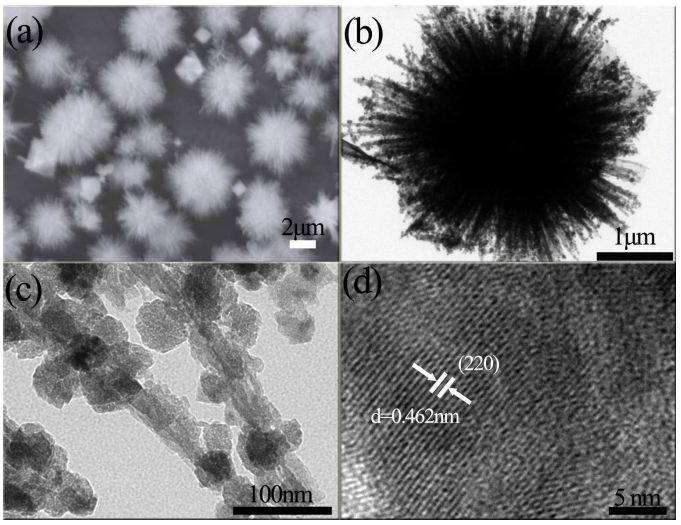


Fig. 2 Characterization of MnS: (a) SEM image of MnS in overall view; (b), (c), and(d) TEM micrographs;

Synthesizing specific material with a regular morphology is known to be difficult. Different from other synthetic methods, which were complicated, time-consuming, and costly[49-51], by contrast, we synthesized dandelion-like MnS with regular micro/nanostructure via a simple method. Given the positive effects of the morphology on the product properties, we introduced part metal ions of the IB group to MnS without changing the morphology via action exchange, and the method was confirmed to have a positive effect on the catalytic performance[52–53]. The stable trivalent state of gold ion was considered but is uneconomical for massive application. In this study, $Cu^{2+}$ and $Ag^{+}$ were chosen for cation exchange with the as-prepared MnS. The experimental results proved that the introduction of beneficial metals regulated the composition of the products without changing the morphology and also improved the catalytic performance of the products. To introduce $Cu^{2+}$ and $Ag^{+}$ to the as-prepared MnS, a series of experiments was designed. $Cu^{2+}$ was selected for ion exchange with the as-obtained MnS. $Cu(NO_3)_2{\bullet}3H_2O$ was selected because $NO_3^-$ decomposes into gas after heating without introducing any impurities into the reaction.

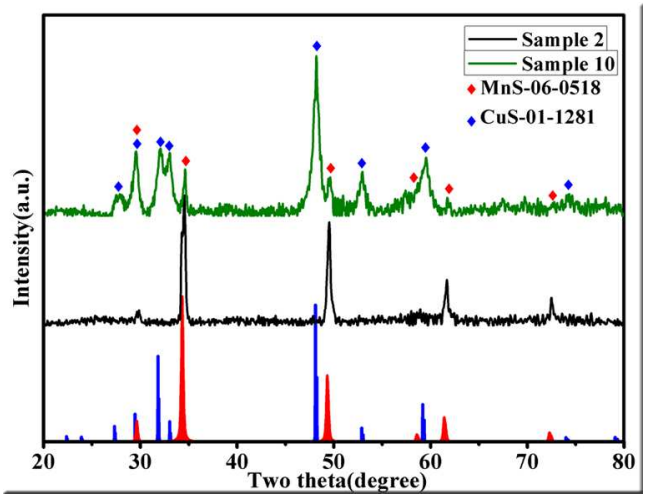


**Figure.3** XRD pattern comparison of Sample **2** and Sample **10**

By investigating the reaction time, reaction temperature, and

reactant concentration, we obtained the optimum cation exchange conditions. In the case of excessive $Cu^{2+}$, a series of products was synthesized by adjusting the reaction time at room temperature. Sample **10** ($Mn_{0.05}Cu_{0.95}S$) was obtained with an MnS : $Cu^{2+}$ ratio of 1:2 at room temperature for 1 h. The catalytic performance of Sample **10** was significantly improved compared with that of the as-prepared MnS. Fig. 3 presents the XRD pattern comparison of Samples **2** and **10**. The XRD pattern of Sample **10** indicated that ion-exchange reaction occurred. The diffraction peaks marked with ♦ matched well with the CuS standard card JCPDS No. 01-1208, and the peaks marked with ♦ corresponded to the MnS standard card JCPDS No. 06-0518.

Samples **3**, **4**, **5**, **6**, **7**, **8**, **9**, and **10** were obtained with an MnS and $Cu(NO_3)_2{\bullet}3H_2O$ ratio of 1:2 at room temperature for 2 min, 5 min, 10 min, 20 min, 30 min, 40 min, 50 min, and 1 h, respectively. Fig. S2 presents the comparison of the XRD patterns. As shown in the graph, the diffraction peaks corresponding to the CuS signals were stronger, whereas those corresponding to the MnS signals were weaker with increasing time. This result indicates that the cation exchange reaction occurred at a greater degree. This phenomenon may be attributed to the lower solubility product constant of CuS than MnS, which made the cation exchange reaction smooth. The increase in reaction time resulted in further enhanced ion-exchange reaction and increased intensity of the peaks corresponding to CuS.

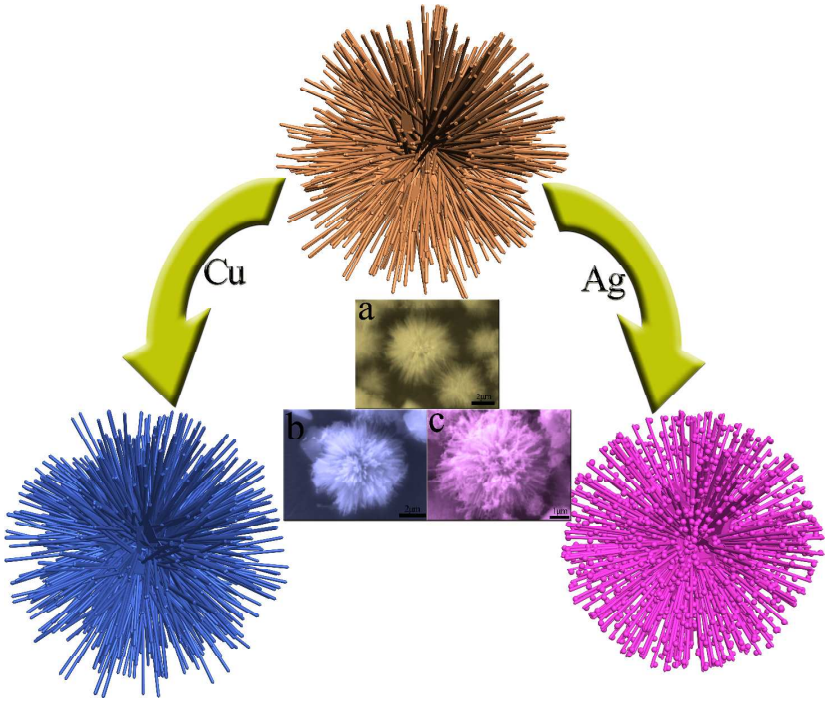


**Figure.4** The Schematic diagram of the morphology transfer between the as-prepared MnS and Sample **10**, **16**. (a) The SEM image of as-prepared MnS; (b) The SEM image of Sample **10**; (c) The SEM image of Sample **16**.

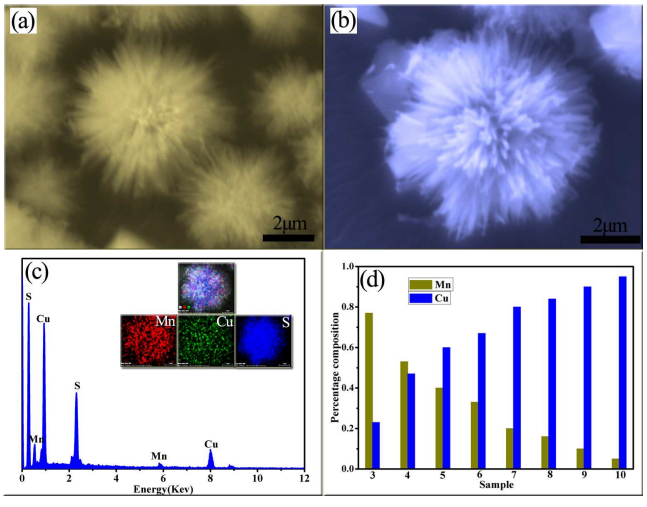


**Figure.5** (a) SEM image of Sample **2**; (b) SEM image of Sample **10**; (c) EDS spectra of Sample **10** and EDS surface scanning images of the sphere section of Sample **10**, (d) the Mn and Cu content changes of the Sample **3**-**10**

In this study, a series of ion exchange reactions was performed to determine the reaction conditions and realize better morphology transfer. To study the effect of reaction time on a reaction, a series of experiments was conducted with an MnS and $Cu(NO_3)_2{\bullet}3H_2O$ ratio of 1:2 at room temperature. We obtained $Mn_{0.77}Cu_{0.23}S$ (Sample **3**), $MnS_{0.53}Cu_{0.47}S$ (Sample **4**), $Mn_{0.40}Cu_{0.60}S$ (Sample **5**), $Mn_{0.33}Cu_{0.67}S$ (Sample **6**), $Mn_{0.20}Cu_{0.80}S$ (Sample **7**), $Mn_{0.16}Cu_{0.84}S$ (Sample **8**), $Mn_{0.10}Cu_{0.90}S$ (Sample **9**), and $Mn_{0.05}Cu_{0.95}S$ (Sample **10**) at reaction times of 2 min, 5 min, 10 min, 20 min, 30 min, 40 min, 50 min, and 1 h, respectively. Fig. 4 shows the schematic diagram of the morphology transfer of the cation exchange reaction. As shown in the graph, the morphology of Sample **10** remained unchanged compared with that of MnS. The SEM image of Sample **10** is presented in Fig. 5b. Compared with the as-prepared

MnS (Fig. 5a), no significant difference was found between the morphology of Samples **10** and **2**. Sample **10** maintained the morphology of MnS to a great extent after the cation exchange reaction. The SEM images of Samples **3**, **4**, **5**, **6**, **7**, **8**, **9**, and **10** are presented in Fig. S3. Fig. S3 shows that the morphology of the as-prepared samples was similar to that of MnS, which may be attributed to the complete reaction between the as-prepared MnS and $Cu^{2+}$. Through the analysis of the cation exchange reaction conditions, this phenomenon may be due to the cation exchange reaction conducted at room temperature, and the mild reaction condition was helpful in the morphology genetic. Therefore, the morphologies of Samples **3**, **4**, **5**, **6**, **7**, **8**, **9**, and **10** were almost the same as MnS, and the successful morphology transfer could be achieved at appropriate reaction conditions.

Fig. 5c shows the EDS image of Sample **10**. EDS surface scanning was performed to verify the element distribution of Sample **10**. The inset in Fig. 5c shows the distribution of Mn, Cu, and S atoms on the surface of Sample **10**, which are marked in red, green, and blue, respectively. As shown in the EDS surface scanning images, Mn, Cu, and S atoms covered the surface of Sample **10**. To characterize the extent change of reaction more precisely via EDX data analysis, the changes in Mn and Cu contents in Samples **3**, **4**, **5**, **6**, **7**, **8**, **9**, and **10** are shown in Fig. 5d. The increase in reaction time resulted in a decrease in Mn content and an increase in Cu content. At a MnS and $Cu^{2+}$ ratio of 1:2, the Cu content increased to 0.23, 0.47, 0.60, 0.67, 0.80, 0.84, 0.90, and 0.95 when the reaction time was 2 min, 5 min, 10 min, 20 min, 30 min, 40 min, 50 min, and 1 h, respectively. Based on the analysis of Cu content in $Mn_xCu_{1-x}S$, at reaction time of 2 min and 5 min to 10 min, the Cu content increased to a relatively large extent, which proved that the cation exchange reaction was violent in the first 10 min. This result is due to the small solubility constant of CuS that impelled the cation exchange reaction further at the beginning, which led to the rapid increase in the Cu content of the product. When the reaction time was increased, the Cu content in $Mn_xCu_{1-x}S$ increased to 0.67, 0.80, 0.84, 0.90, and 0.95. Although the Cu content increased, the incremental extent was small compared with those in Samples **3**, **4**, and **5**. This finding may be attributed to the decreasing reactant concentration that led to the decrease in reaction rate, and the increase in the Cu content was not noticeable.

Based on the aforementioned discussion, a series of $Mn_xCu_{1-x}S$ was synthesized by controlling the reaction time. The SEM images of as-prepared products were characterized, and the morphology of good-shaped dandelion-like MnS was transferred to the follow-up products after the cation exchange reaction. Meanwhile, the XRD patterns and EDX data proved the occurrence of the cation exchange reaction.

The good results of the cation exchange reaction between the as-prepared MnS and the $Cu^{2+}$ were used to investigate the composition adjustment of the products by changing the center metal ions. Considering that $Ag^+$ and $Cu^{2+}$ belong to the same subgroup in the periodic table of elements and have a similar property, another series of experiments was conducted using the as-prepared MnS and $Ag^+$. $AgNO_3$ was selected because $NO_3^-$ does not introduce any impurities into the reaction. In the premise of the aforementioned conditions, Samples **11**, **12**, **13**, **14**, **15**, and **16** were synthesized by the reaction of the as-prepared MnS and the $AgNO_3$ aqueous solution at room temperature for 2, 4, 5, 10, 20, and 30 min, respectively. Sample **16** was synthesized with an MnS and $Ag^+$ ratio of 1:1 at room temperature for 30 min.

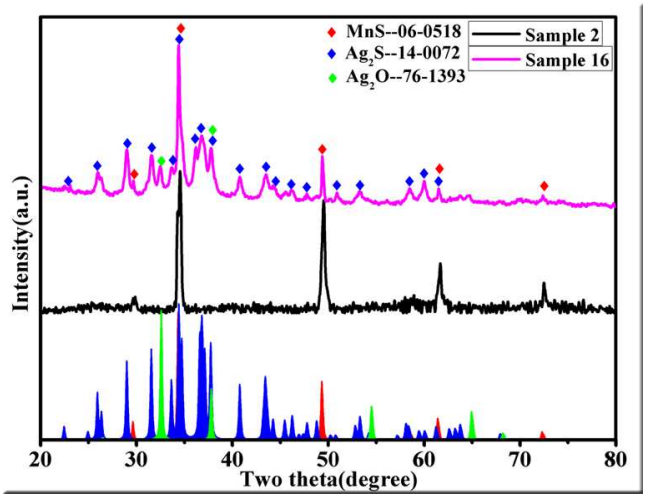


**Fig.6** XRD pattern of as-prepared Sample **2** and **16**

The XRD pattern of sample **16** is shown in Fig. 6. As shown in the graph, the diffraction peaks of the XRD pattern of the as-prepared sample **16** marked with ♦ matched well with the $Ag_2S$ standard card JCPDS No. 14-0072, which confirmed that the ion-exchange reaction occurred. The diffraction peaks marked with ♦ corresponded to the MnS standard card JCPDS No. 06-0518. In addition, the diffraction peaks of the XRD pattern marked with ♦ matched with the $Ag_2O$ standard card JCPDS No. 76-1393. The cation exchange reaction occurred with distilled water as the solvent, and AgOH existed at the beginning of the reaction and decomposed into $Ag_2O$. Compared with the diffraction peaks of $Ag_2S$, those of $Ag_2O$ were less and weaker. Fig. S4 shows the XRD patterns of Samples **11**, **12**, **13**, **14**, and **15**. As presented in the graph, the increased reaction time weakened the diffraction peaks of $Ag_2O$ and gradually strengthened the diffraction peaks of $Ag_2S$. This result was attributed to the lower solubility constant of $Ag_2S$ than $Ag_2O$, which made the exchange reaction beneficial to $Ag_2S$ formation. Moreover, the diffraction peaks corresponding to $Ag_2S$ signals were stronger with increasing time, which indicates that the ion-exchange reaction occurred at a greater degree.

The SEM images of MnS and Sample **16** are shown in Figs. 7a and 7b, respectively. Sample **16** kept the dandelion-like structure of MnS. Fig. 4 shows the schematic diagram of the morphology genetic of the cation exchange reaction. As shown in the graph, the morphology of the as-prepared Sample **16** was similar to that of MnS (Fig. 7a). The difference was the presence of minute particles on Sample **16** compared with as-prepared MnS. The EDS analysis results of the particles and the needle-like structure are shown in Fig. S5; the characterization results show that their composition was the same. The small change in Sample **16** may be due to the violent cation exchange reaction between MnS and $Ag^+$, which hindered morphology transfer. To investigate the effects of reaction time on the product, $Mn_{0.80}Ag_{0.40}S$ (Sample **11**), $Mn_{0.73}Ag_{0.54}S$ (Sample **12**), $Mn_{0.58}Ag_{0.84}S$ (Sample **13**), $Mn_{0.53}Ag_{0.94}S$ (Sample **14**), $Mn_{0.52}Ag_{0.96}S$ (Sample **15**), and $Mn_{0.48}Ag_{1.04}S$ (Sample **16**) were

synthesized with an MnS and $AgNO_3$ ratio of 1:1 at room temperature for 2, 4, 5, 10, 20, and 30 min, respectively. Fig. S6 shows the SEM images of the as-prepared products. An increase in reaction time resulted in almost no change in the morphologies of the samples; the basic microsphere of the MnS was maintained very well. This result was mainly due to the mild reaction conditions and the appropriate concentration of the reactants.

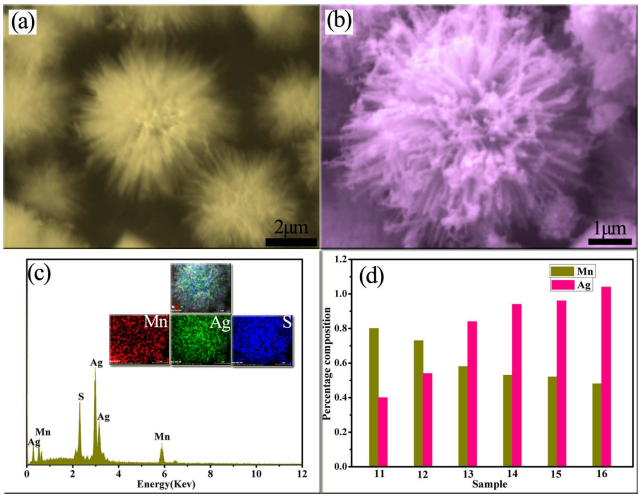


**Figure.7** (a) SEM image of Sample **2**; (b) SEM image of Sample **16**; (c) EDS spectra of Sample **16** and EDS surface scanning images of the sphere section of Sample **16**, (d) the Mn and Ag content changes of the Sample **11**-**16**

Fig. 7c shows the EDS image of Sample **16**. The element distribution of Sample **16** was characterized *via* EDS surface scanning. The inset in Fig. 7c shows the distribution of Mn, Ag, and S atoms on the surface of Sample **16**, which are marked in red, green, and blue, respectively. The EDS surface scanning images showed that the Mn, Ag, and S atoms covered the surface of Sample **16**. Fig. 7d shows the EDX data analysis of Mn and Ag content changes of the as-prepared Samples **11**, **12**, **13**, **14**, **15**, and **16**. With increasing reaction time, the Mn content decreased and the Ag content increased. In the as-prepared Samples **11**, **12**, **13**, **14**, **15**, and **16**, the Ag content increased to 0.20, 0.27, 0.42, 0.47, 0.48, and 0.52 when the reaction time was 2, 4, 5, 10, 20, and 30 min, respectively. In the first 10 min of the cation exchange reaction, the Ag content increased to a relatively large extent, but at the last 20 min of the cation exchange reaction, the incremental extent of Ag was small compared with those of Samples **11**, **12**, and **13**. In contrast to the change in the Cu content in $Mn_xCu_{1-x}S$, the Ag content remained stable in the last 20 min of reaction. This result may be due to $Ag_2O$ formation that impeded the reaction between $Ag^+$ and the as-prepared MnS, which made the cation exchange reaction reach equilibrium.

Based on the results and discussion, $Mn_yAg_{2(1-y)}S$ maintained the morphology of MnS after the cation exchange reaction, which determined the morphology genetic from MnS to the as-prepared subsequent products. Meanwhile, the XRD patterns and EDX data proved the occurrence of the cation exchange reaction.

The as-prepared dandelion-like MnS and part of the products synthesized via cation exchange reaction were used as catalysts for the degradation of MB and RB molecules because of their special hierarchical structures. The corresponding experiments were carried out with the addition of $H_2O_2$. In our experiment, $H_2O_2$ yielded highly reactive hydroxyl radicals that could oxidize MB into smaller molecules ($CO_2$, $H_2O$, etc.). The catalytic properties of the samples were closely associated with the amount of hydroxyl radicals. The rate of $H_2O_2$ alone to degrade the dye solutions was very slow[54] without the assistance of a catalyst. Moreover, only the as-prepared products as catalysts do not contribute to the catalytic process. The catalytic properties of the as-prepared products were investigated based on their UV–vis absorption spectra, as shown in Fig. 8. The figure shows the efficient catalysis of $H_2O_2$ to release hydroxyl radicals (•OH) and to degrade MB and RB molecules in a short time. A brief description of the reaction mechanism of Samples **3**, **4**, **5**, **6**, **7**, **8**, **9**, and **10** is described as follows[55].

$$M^{x+} + H_2O_2 \rightarrow H^+ + MOOH^{(x-1)+}$$
$$MOOH^{(x-1)+} \rightarrow HOO^- + M^{(x-1)+}$$
$$M^{(x-1)+} + H_2O_2 \rightarrow M^{x+} + OH^- + OH^-$$

$HO^-$ radicals can attack an organic substrate, RH, such as MB and RB, as follows:

$$RH + HO^- \rightarrow R^- + H_2O$$

In this study, the as-prepared dandelion-like MnS was used as a template to synthesize the cation exchange reaction products. The as-prepared cation exchange reaction products almost retained the morphology of MnS. The needle-like hierarchical structure of the as-prepared products was postulated to improve the catalytic performance because of larger specific surface area and more active sites. Fig. 8 displays the changes in the UV–vis spectra during the removal of MB and RB molecules by Samples **2**, **10**, and **16**. The degradation curves of MB and RB by the as-prepared MnS microspheres are shown in Figs. 8a and 8b, respectively. Fig. 8a displays the changes in the UV–vis spectra during the removal of MB molecules by Sample **2**. The decolorization degree of the aqueous MB reached 18% after 10 min and 65% after 30 min. After 60 min, the decolorization degree reached 97%, and decolorization was maintained at a stable level after 60 min. Fig. 8b shows the changes in the UV–vis spectra during the removal of RB molecules by Sample **2**. The decolorization degree of the aqueous RB reached 16% after 10 min and 68% after 40 min. After 80 min, the decolorization degree reached 98%, which was the same as that of the aqueous MB. This decolorization was stably maintained after 80 min.

The as-prepared cation exchange reaction samples were also used to examine catalytic performance. For example, the changes in the UV–vis spectra in Sample **10** during the removal of MB and RB molecules by Sample **10** are shown in Figs. 8c and d, respectively. Fig. 8c shows that the decolorization degree of the aqueous RB reached 72% after 2 min, and at a catalytic time of 8 min, MB degradation was almost completed. Compared with the as-prepared MnS, the efficiency for the MB degradation of Sample **10** was greatly improved. This result may be attributed to the highest content of CuS in Sample **10**, based on the aforementioned discussion of the catalytic reaction mechanism. CuS had a positive effect on the catalytic reaction, which greatly reduced the degradation time of MB. This finding was also reflected in the discussions of Samples **3**, **4**, **5**, **6**, **7**, **8**, and **9**. The changes in the UV–vis spectra during the removal of MB molecules by Samples **3**, **4**, **5**, **6**, **7**, **8**, and **9** are shown in Fig. S7. The increase in the Cu content in the products resulted in reduced

time for MB degradation. As shown in the diagram, the degradation time of MB by Samples **3** and **4** was at least 16 min. This result was caused by the relatively small Cu content of Samples **3** and **4**, and the catalytic effect was not noticeable compared with that in Sample **10**. In Sample **5**, when the Cu content was increased to 0.6, the complete degradation time of MB was 14 min, which was reduced to 2 min compared with those of Samples **3** and **4**. The time for the complete degradation of MB by Samples **6**, **7**, and **8** was 12 min. No significant difference in Cu content was observed in Samples **6**, **7**, and **8**, and the degradation degree of MB was similar. When the Cu content was increased to 0.9, the complete degradation time of MB was 10 min. The changes in the UV–vis spectra during the removal of RB molecules by Samples **3**, **4**, **5**, **6**, **7**, **8**, and **9** are shown in Fig. S8. Similar to MB degradation, the degradation time of RB was reduced along with the increase in Cu content in Samples **3**, **4**, **5**, **6**, **7**, **8**, **9**, and **10**. Thus, we conclude that the catalytic efficiency is proportional to the degree of the cation exchange reaction.

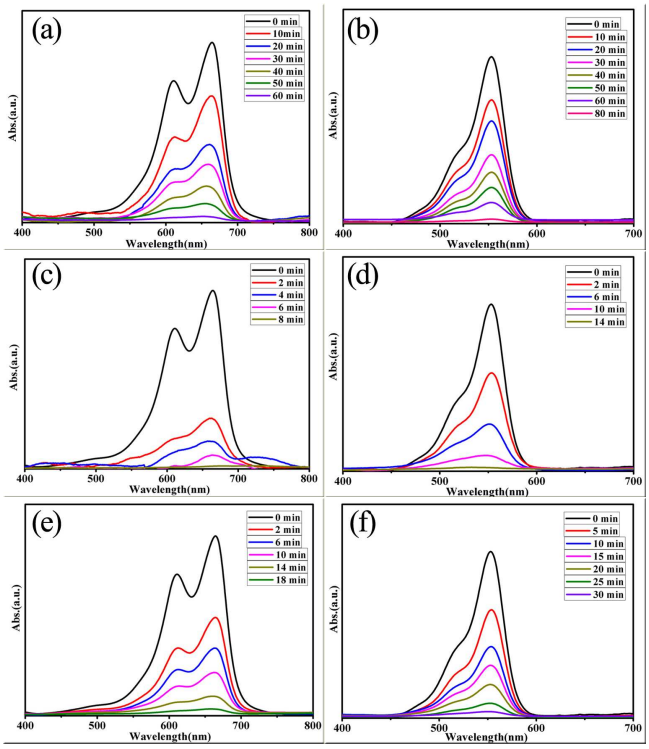


**Fig. 8** Changes in the UV-vis spectra during the removal of (a) MB by Sample **2**; (b) RB by Sample **2**; (c) MB by Sample **10**; (d) RB by Sample **10**; (e) MB by Sample **16**; (f) RB by Sample **16**.

Based on the catalytic discussion of $Mn_xCu_{1-x}S$, the changes in the UV–vis spectra during the removal of MB and RB molecules by Sample **16** are shown in Figs. 8e and f, respectively. Fig. 8e shows that the decolorization degree of the aqueous MB reached 48% after 2 min and 95% after 18 min. The decolorization was stably maintained after 18 min. In Fig. 8f, the degradation degree of the aqueous RB was examined every 5 min. The degradation degree was 24% at the first 5 min. It reached 68% after 15 min and was almost complete after 30 min. The catalytic reaction then reached equilibrium. In addition, in the same experimental condition, we tested the catalytic performance of the P25. The degradation curves of MB and RB by the P25 are shown in FigS9a and FigS9b, respectively. As shown in the Fig. 9S, the complete degradation time of MB was 130 min, and the complete degradation time of RB was 180 min. Though the analysis of the experimental results, compared with P25, the as-prepared MnS, $Mn_xCu_{1-x}S$ and $Mn_yAg_{2(1-y)}S$ shown higher catalytic performance.

## Conclusions

In summary, large-scale dandelion-like MnS was successfully synthesized with manganese complex as a template via a facile and environmentally friendly approach. The structure and morphology of MnS could be controlled in a stable level by adjusting the reaction temperature and time. The manganese complex was synthesized via a simple method by using low-cost chemical raw materials. $Cu^{2+}$ and $Ag^{+}$ were introduced to the as-obtained MnS as beneficial metals via cation exchange at room temperature. The results of the cation exchange reaction showed that the morphology of the as-prepared MnS was transferred to $Mn_xCu_{1-x}S$ and $Mn_yAg_{2(1-y)}S$. This result provides information for the synthesis of inorganic nanomaterials and determined resource maximization. The needle-like structure of the as-prepared products provided a large specific surface area and more active sites, which could improve the catalytic performance. The introduction of beneficial metals improved the catalytic efficiency in degrading dye-containing solutions, such as MB and RB, to a great extent compared with that of the as-prepared MnS. The catalytic efficiencies of $Mn_xCu_{1-x}S$ and $Mn_yAg_{2(1-y)}S$ were improved by six and three times, respectively, compared with that of the as-prepared MnS. Furthermore, compared with the P25 (Fig. S9), the as-prepared MnS, $Mn_xCu_{1-x}S$ and $Mn_yAg_{2(1-y)}S$ shown higher catalytic performance in same experimental conditions. The comprehensive analysis indicated that the composition and performance of the products could be adjusted by changing the central metal ion without changing the morphology.

## Notes and references

[a] *Center For Advanced Functional Materials Research, Zhongyuan University of Technology, Henan 450007, P. R. China. E-mail: mlwzzu@163.com*
[b] *Department of Chemistry, Zhengzhou University, Henan 450001, P. R. China. E-mail: chenweih@zzu.edu.cn*
[c] *Key Laboratory for Micro-Nano Energy Storage and Conversion Materials of Henan Province, Institute of Surface Micro and Nano Materials, Xuchang University, Henan 461000, P. R. China.*
† Electronic Supplementary Information (ESI) available: [Figure S1~ S7: SEM images, XRD patterns, EDS analysis data, and catalysis properties of MnS and its ion exchanged sample]. See DOI: 10.1039/b000000x/

1. P. Collier and C. M. Alles, *Science*, 2010, **330**, 919.
2. Y. J. Wang, D. G. Chen, Y. D. Wang, F. Huang, Q. C. Hu and Z. Lin, *Nanoscale*, 2012, **4**, 3665.
3. Y. Zushi, F. Ye, M. Motegi, K. Nojiri, S. Hosono, T. Suzuki, Y. Kosugi, K. Yaguchi and S. Masunaga, *Environ. Sci. Technol*, 2011, **45**, 2887.
4. K. Pakshirajan and S. Singh, *Ind. Eng. Chem. Res*, 2010, **49**, 7484.
5. N. M. Mahmoodi, B. Hayati, M. Arami and F. Mazaheri, *J. Chem. Eng. Data*, 2010, **55**, 4660.

6. A. Rodriguez, G. Ovejero, J. L. Sotelo, S. M. Mestanza and J. Garcia, *Ind. Eng. Chem. Res*, 2010, **49**, 498.
7. G. Crini, *Bioresour. Technol*, 2006, **97**, 1061.
8. Y. M. Han, J. J. Cao, F. Wu, B. C. Zhang, C. L. Zhan, C. Wei and Z. Z. Zhao, *J. Environ. Monit*, 2012, **14**, 2762.
9. Y. Y. Yu, Q. X. Huang, Z. F. Wang, K. Zhang, C. M. Tang, J. L. Cui, J. L. Feng and X. Z. Peng, *J. Environ. Monit*, 2011, **13**, 871.
10. L. Jones, B. Kinsella, A. Furey and F. Regan, *J. Environ. Monit*, 2012, **14**, 3009.
11. J. R. Raji and K. Palanivelu, *Idn. Eng. Chem. Res*, 2011, **50**, 3130.
12. D. Valero, J. M. Ortiz, E. Expσsito, V. Montiel and A. Aldaz, *Environ. Sci. Technol*, 2010, **44,** 5182
13. X. Zhuang, Y. Wan, C. M. Feng, Y. Shen and D. Y. Zhao, *Chem. Mater*, 2009, **21,** 706
14. A. Santos, P. Yustos, S. Rodriguez, E. Simon and A. Romero, *Ind. Eng. Chem. Res*, 2010, **49,** 5583
15. C. L. Lim, N. Morad, T. T. Teng and N. Ismail, *J. Hazard. Mater*, 2009, **168,** 383
16. A. Y. Satoh, J. E. Trosko and S. J. Masten, *Environ. Sci. Technol*, 2007, **41**, 2881.
17. H. B. Wu, H. Pang and X. W. Lou, *Energy Environ. Sci*, 2013, **6**, 3619.
18. L. F. Liu, X. D. Ding, J. Li, T. Lookman and J. Sun, *Nanoscale*, 2014, DOI: 10. 1039/C3NR05258C.
19. T. Todd, Z. P. Zhen, W. Tang, H. M. Chen, G. Wang, Y. J. Chuang, K. Deaton, Z. W. Pan and J. Xie, *Nanoscale*, 2014, DOI: 10. 1039/C3NR05623F.
20. N. Wang, D. G. Wang, M. R. Li, J. Y. Shi and C. Li, *Nanoscale*, 2014, DOI: 10. 1039/C3NR05601E.
21. D. Ding, X. X. Li, S. Y. Lai, K. Gerdes and M. L. Liu, *Energy Environ. Sci*, DOI: 10. 1039/C3EE42926A.
22. H. H. Li, C. H. Cui, S. Zhao, H. B. Yao, M. R. Gao, F. J. Fan and S. H. Yu, *Adv. Energy Mater*, 2012, **2**, 1182.
23. C. B. Quyang, X. M. Qian, K. Wang and H. B. Liu, *Dalton Trans*, 2012, **41**, 14391
24. Y. Z. Fan, R. M. Liu, K. W. Du, Q. Y. Lu, H. Pang and F. Gao, *J. Mater. Chem*, 2012, **22**, 12609.
25. J. W. Shi, J. H. YE, Q. Y. Li, Z. H. Zhao, H. Tong, G. C. Xi and L. J. Guo, *Chem. Eur. J*, 2012, **18**, 3157
26. Y. Shemesh, J. E. Macdonald, G. Menagen and U. Banin, *Angew. Chem. Int. Ed*, 2011, **123**, 1217
27. X. C. Duan, J. Q. Yang, H. Y. Gao, J. M. Ma, L. F. Jiao and W. J. Zheng, *CrystEngComm*, 2012, **14**, 4196
28. S. Senapati, S. K. Srivastava, S. B. Singh and H. N. Mishra, *J. Mater. Chem*, 2012, **22**, 6899
29. L. L. Wang, H. X. Gong, C. H. Wang, D. K. Wang, K. B. Tang and Y. T. Qian, *Nanoscale*, 2012, **4**, 6850
30. N. Meir, I. J.-L. Plante, K. Flomin, E. Chockler, B. Moshofsky, M. Diab, M. Volokh and T. Mokari, J. *Mater Chem. A*, 2013, **1**, 1763
31. X. J. Bian, W. N. Sun and C. Wang, *Dalton. Trans*, 2013, **42**, 14006
32. Z. Q. Liu, W. Y. Huang, Y. M. Zhang and Y. X. Tong, *CrystEngCom*, 2012, **14**, 8621
33. Z. G. Cheng, S. Z. Wang, Q. Wang and B. Y. Geng, *CrystEngCom*, 2010, **12**, 144
34. H. H. Li, C. H. Cui, S. Zhao, H. B. Yao, M. R. Gao. F. J. Fan and S. H. Yu, *Adv. Energy Mater*, 2012, **2**, 1182
35. M. F. Wang, F. X, W. J. Li, M. F. Chen and Y. Zhao, *J. Mater Chem. A*, 2013, **1**, 8616
36. X. G. Ding, Y. Zou, F. Ye, J. Yang and J. Jang, *J. Mater Chem. A*, 2013, **1**, 11880
37. R-X Yao, X. Xu and X-M Zhang, *Chem. Mater*, 2012, **24,** 303
38. S. H. Yang, G. S. B. Martin, J. J. Titman, A. J. Blake, D. R. Allan, N. R. Champness and M. Schröder, *Inorg. Chem*, 2012, **124,** 921
39. B. J. Beberwyck and A. P Alivisatos, *J. Am. Chem. Soc*, 2012, **134**, 19977
40. J. Liao, H. Li, W. Z. Zeng, D. B. Sauer, R. Belmares and Y. X. Jiang. *Science*, 2012, **335**, 686..
41. E. Q. Procopio, F. Linares, C. Montoro, V. Colombo, A. Maspero, E. Barea and J. A. R. Navarro, *Angew. Chem. Int. Ed*, 2010, **122**, 7466.
42. J. S. Li, T. R. Zhang, J. P. Ge, Y. D. Yin and W. W. Zhong, *Angew. Chem. Int. Ed*, 2009, **121**, 1616.
43. M. V. Kovalenko, D. V. Talapin, M. A. Loi, F. Cordella, G. Hesser, M. I. Bodnarchuk and W. Heiss, *Angew. Chem. Int. Ed*, 2008, **120**, 3071.
44. R. D. Robinson, B. Sadtler, D. O. Demchenko, C. K. Erdonmez, L. W. Wang and A. P. Alivisatos. *Science*, 2007, **317**, 355.
45. D. H. Son, S. M. Hughes, Y. D. Yin and A. P. Alivisatos. *Science*, 2004, **306**, 1009
46. M. Nagarathinam, J. L. Chen and J. J. Vittal, *Crystal Growth & Design*, 2009, **9**, 2457
47. X. L. Wang, Z. C. Feng, D. Y. Fan, F. T. Fan and C Li, *Crystal Growth &. Design*, 2010, **12**, 5313
48. M. Nagarathinam, J. Chen and J. J. Vittal, *Crystal Growth &. Design*, 2009, **9**, 2457
49. R. Loganathan, S. Ramakrishnan, E. Suresh, M. Palaniandavar, A. Riyasdeen and M. A. Akbarsha, *Dalton Trans*, 2014, DOI: 10. 1039/C3DT52518J
50. M. Yoshida, K. Kinoshita and K. Namba, *Org. Biomol. Chem*, 2014, DOI: 10. 1039/c3ob4251oj
51. R. R. Gowda and E. Y.-X. *Chen, Org. Chem. Front*, 2014, DOI: 10. 1039/c3qo00089c
52. L. W. Mi, W. T. Wei, Z. Zheng, Y. Gao, Y. Liu, W. H. Chen and X. X. Guan, *Nanoscale*, 2013, **5**, 6589
53. Y. J. Ye, J. Chen, Q. Q. Ding, D. Y. Lin, R. L. Dong, L. B. Yang and J. H. Liu, *Nanoscale*, 2013, **13**, 5887
54. Z. Li, L. W. Mi, W. H. Chen, H. W. Hou, C. T. Liu, H. L. Wang, Z. Zheng and C. Y. Shen, *CrystEngComm*, 2012, **14**, 3965
55. T. Rhadfi, J. Y. Piquemal, L. Sicard, F. Herbst, E. Briot, M. Benedetti and A. Atlamsani, *Appl. Cat. A*, 2010, **386**, 132

SYNOPSIS TOC